Supplementary Information

Comparative approaches to understanding speciation: a case study in *Xantusia* lizards

Sonal Singhal, Hayden R. Davis, Julio A. Lemos-Espinal, Matthew K. Fujita, Adam D. Leaché

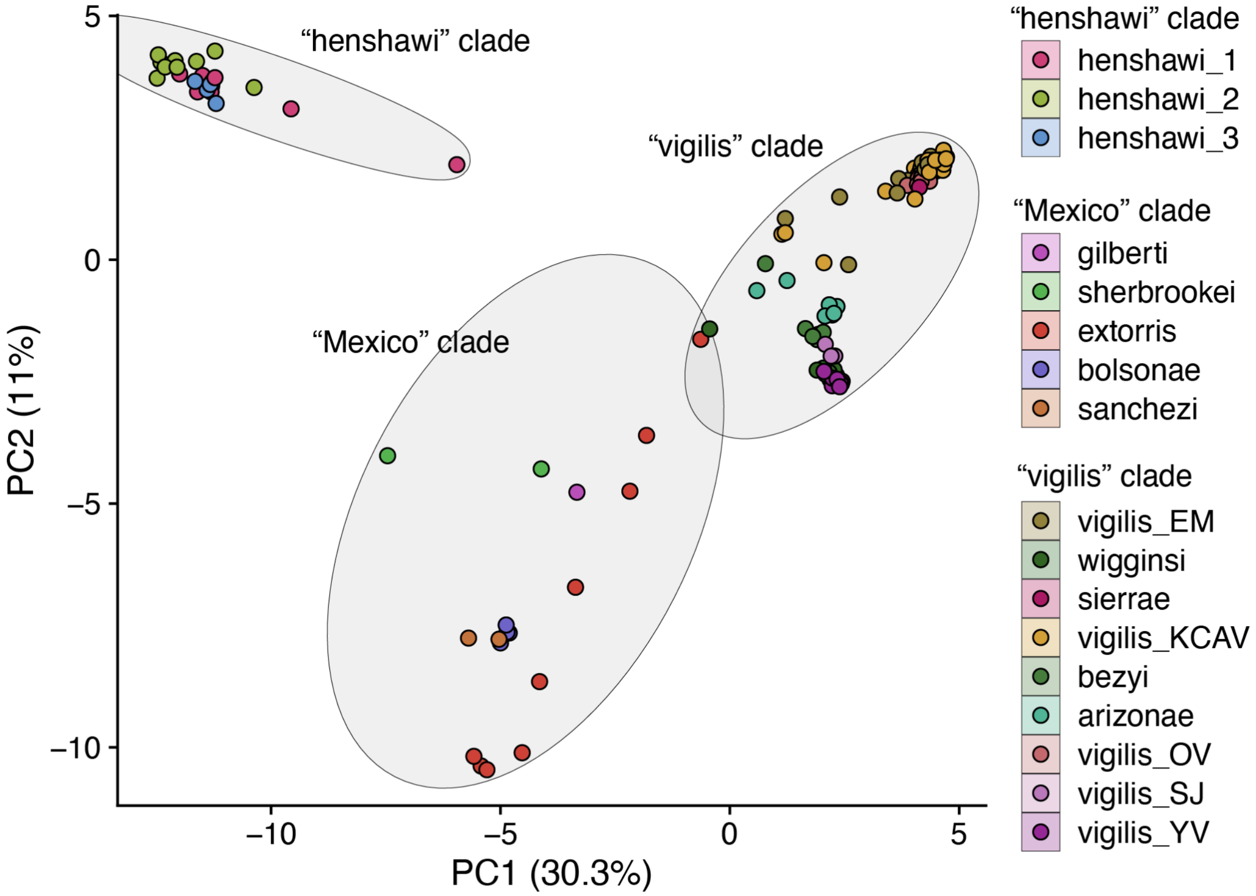

Figure S1: Principal component analysis (PCA) of *Xantusia*. Variants used in PCA were first filtered for completeness (>70%) and minor allele count ≥2; we retained only one variant per locus (*n* = 2,357). *Xantusia* consists of three primary groups (highlighted by gray ellipses; grouped in the legend), which correspond to the major clades seen in the nuclear phylogeny (Fig. 2).

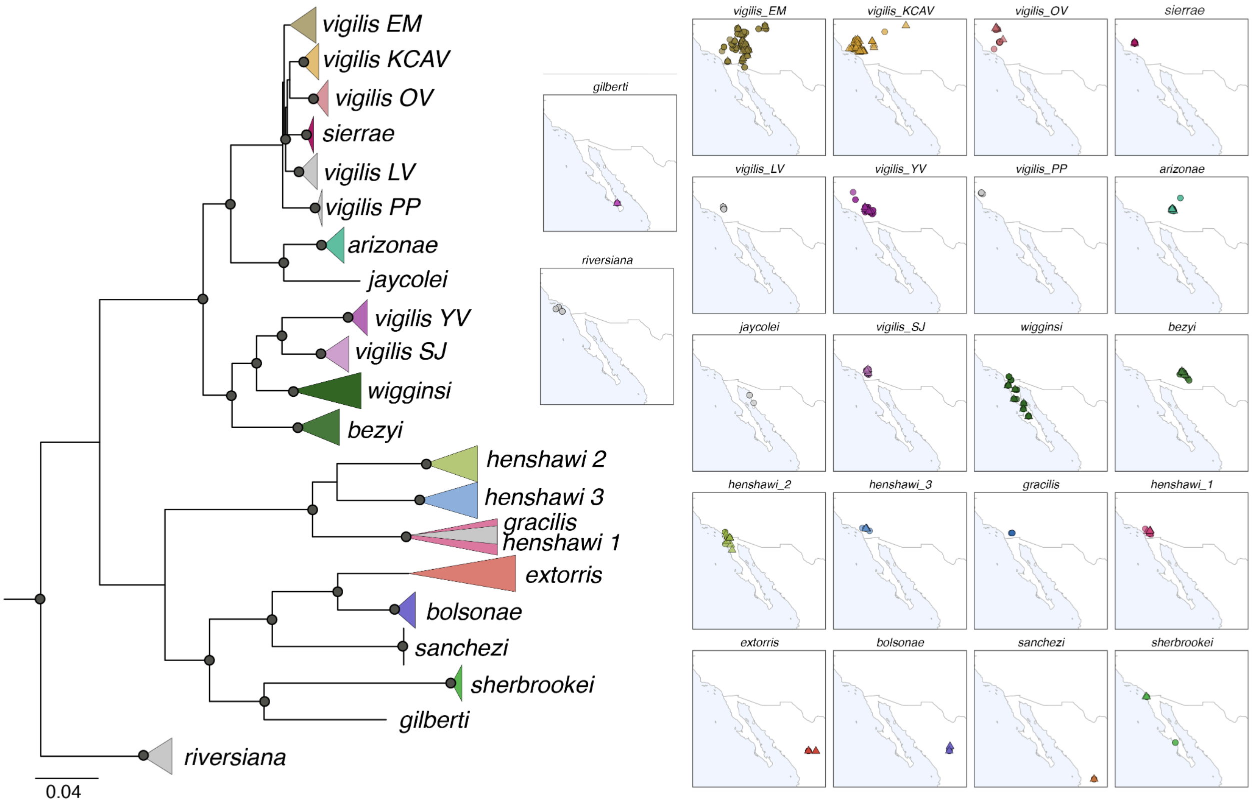

Figure S2: Mitochondrial gene tree for *Xantusia*. Clades are collapsed by operational taxonomic unit (OTU) for ease of visualization. Nodes marked by a dark gray circle have bootstrap support ≥95. Colors follow Figure 2; OTUs shown in gray were not included in our nuclear genomic data set. Maps show distribution of individuals collected for nuclear (shown by triangles) and mitochondrial (shown by circles) data. The genetic structure and evolutionary relationships in *Xantusia* are highly similar across the mitochondrial and genomic-level datasets.

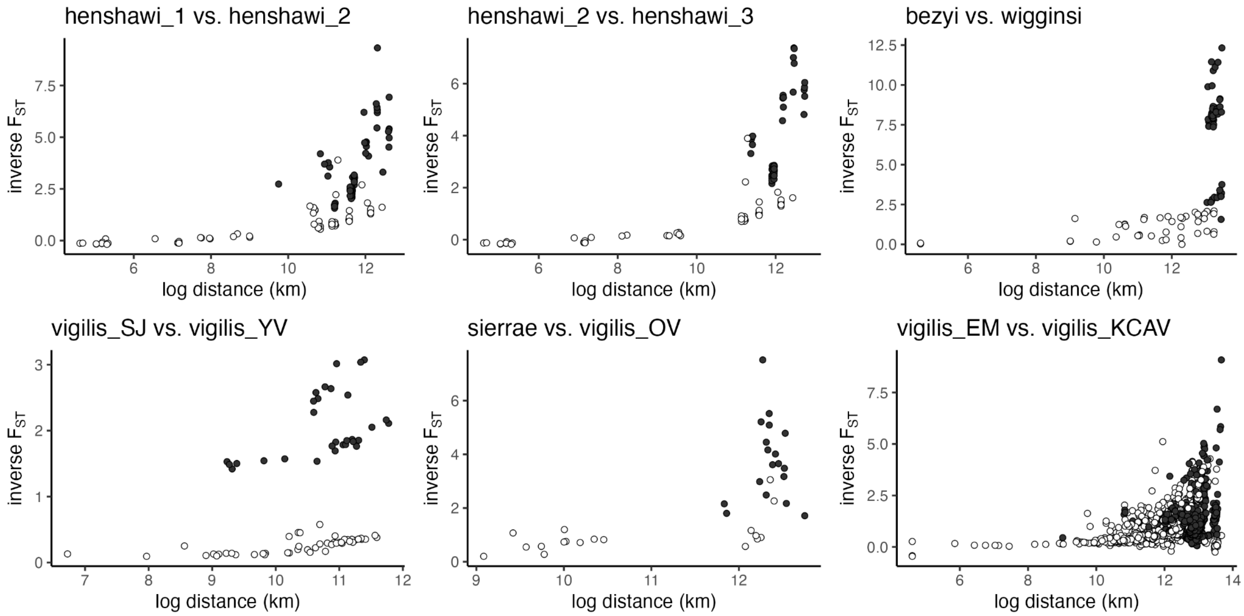

Figure S3: Isolation-by-distance (IBD) patterns within-operational taxonomic units (OTUs) (shown in white) versus between OTUs (shown in black) in *Xantusia* lizards. Inverse F_{ST} is calculated as F_{ST} / (1 - F_{ST}). We only show OTU comparisons that involve putative new lineages or for which lineage uniqueness is ambiguous. Discontinuities in IBD patterns within-OTU versus between-OTUs indicates probable evolutionary independence, as seen in all OTU comparisons but *X. vigilis* EM versus *X. vigilis* KCAV.

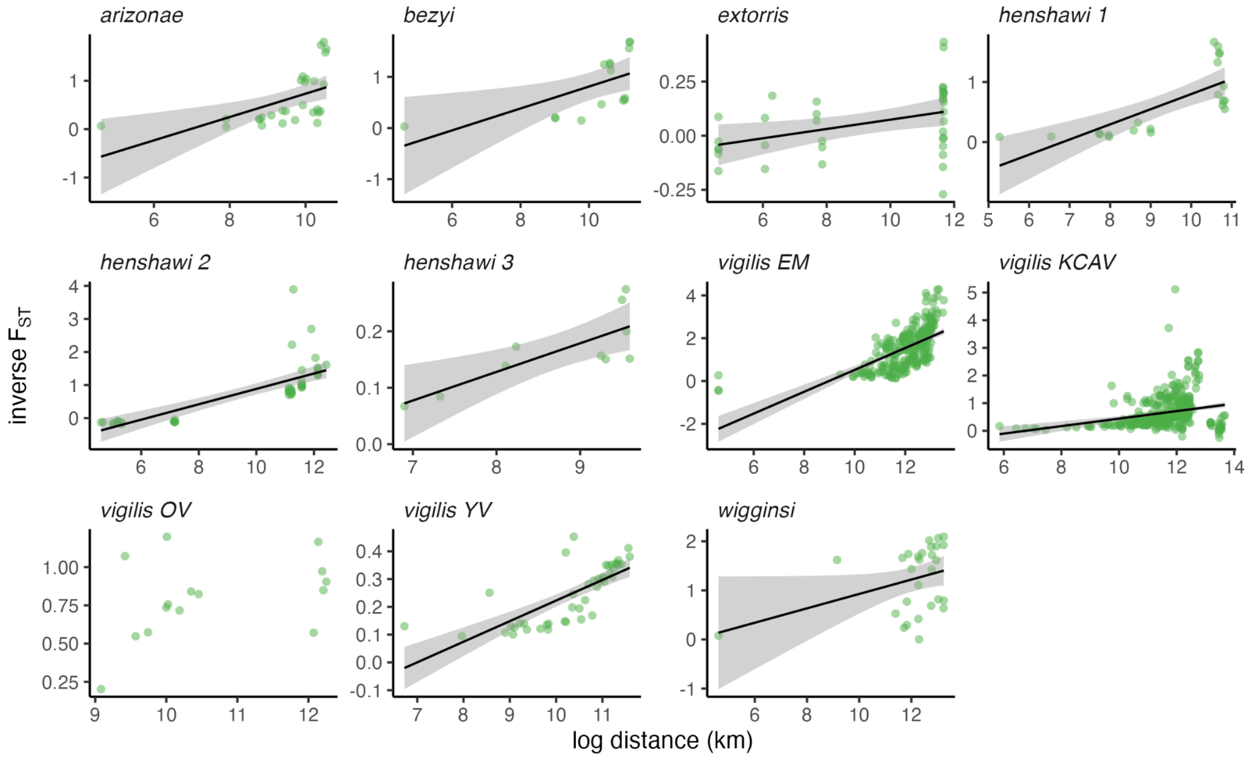

Figure S4: Isolation-by-distance (IBD) patterns shown for pairwise individual comparisons within operational taxonomic units (OTUs). OTUs for which we sampled fewer than four unique localities not shown (*X. bolsonae*, *X. gilberti*, *X. sanchezi*, *X. sherbrookei*, *X. sierrae*, and *X. vigilis* SJ). We show the IBD trend line for those OTUs where the relationship between genetic divergence (inverse F_{ST} or F_{ST} / [1 - F_{ST}]) and geographic distance (log distance in kilometers) is significant (as inferred using a Mantel test).

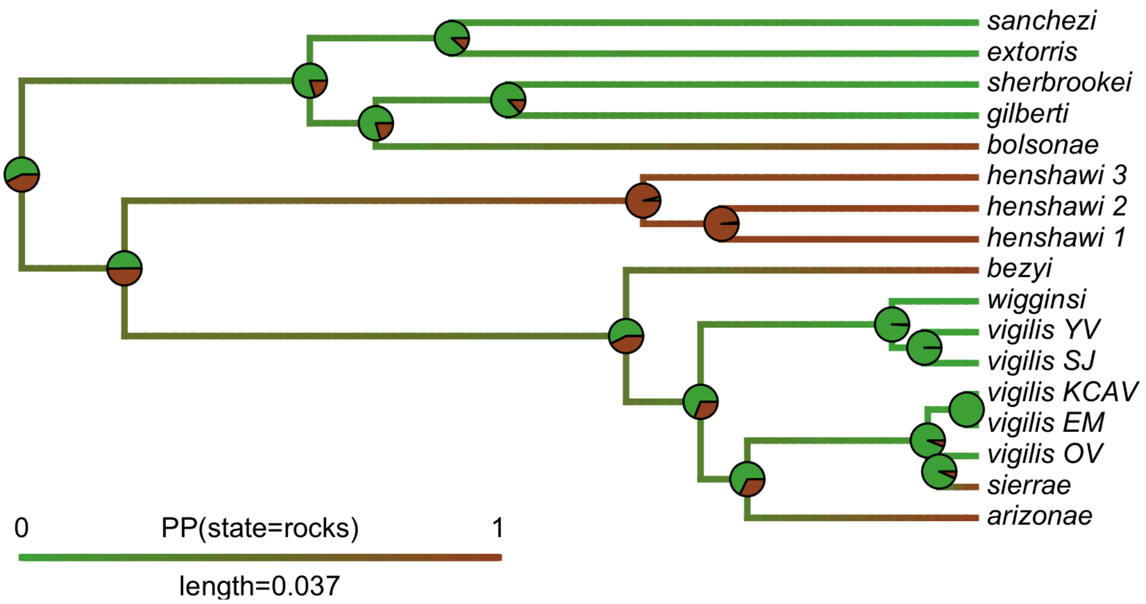

Figure S5: Ancestral state reconstruction of ecomorph across the *Xantusia* phylogeny using stochastic character mapping; brown and green represent rock and plant ecomorphs, respectively. While the primary analysis presented in the text mapped the evolution across a sample of 1000 trees from the posterior, here we show mapping of 1000 simulations across the consensus species tree. On average, we estimate 6.7 transitions between ecomorph types along this species tree.

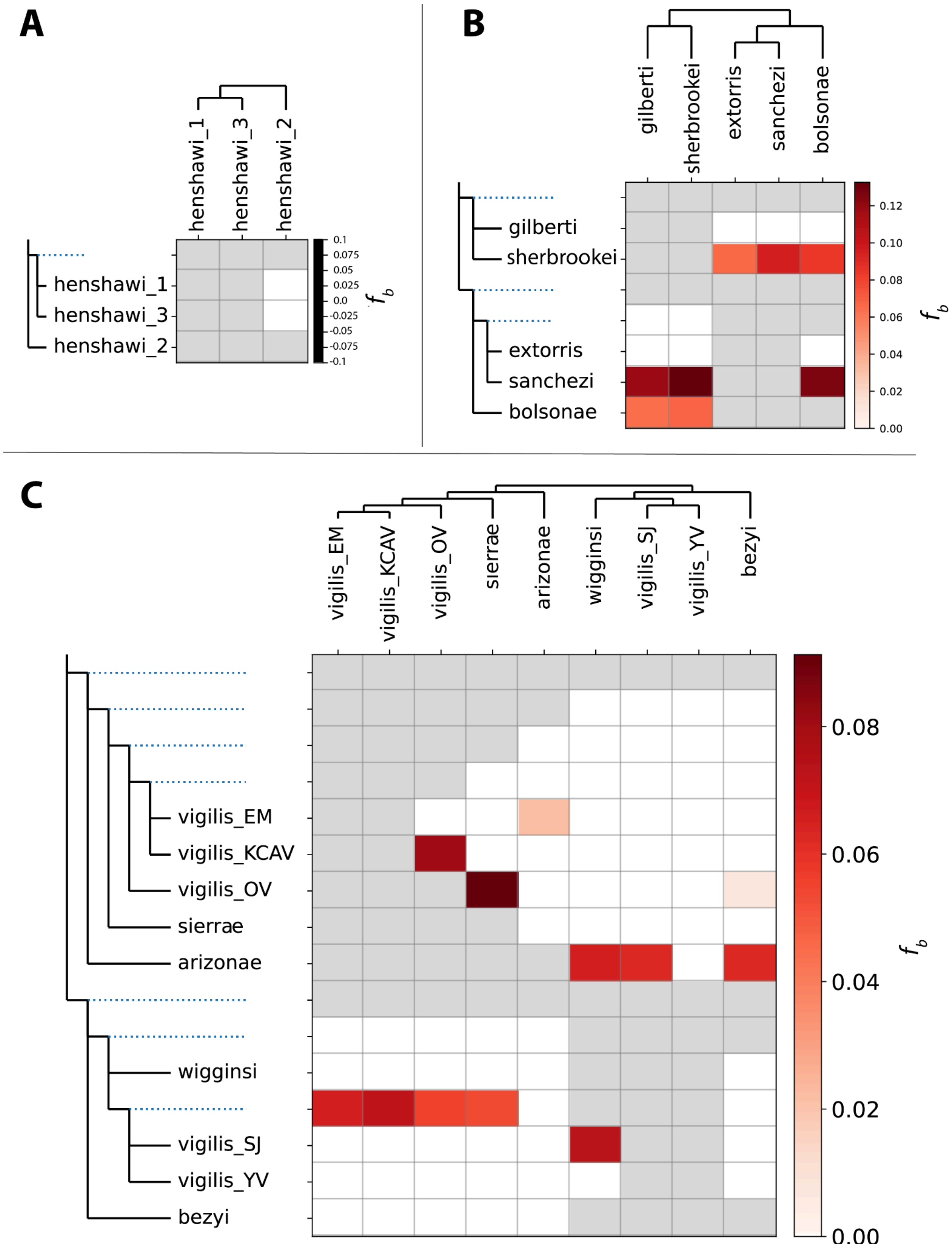

Figure S6: D-statistic results across the three major clades in *Xantusia*. The d-statistic evaluates patterns of shared polymorphisms across triplet species to determine the likelihood of introgression versus incomplete lineage sorting. Here, we calculated the d-statistic across all possible trios and summarized patterns using the f-branch statistic (f_b). The f-branch statistic accounts for correlated patterns of d-statistic that can emerge when an ancestral branch is involved in an introgression event. Dotted blue lines represent internal ancestral branches, and grayed boxes are comparisons for which we could not calculate the d-statistic given the structure of the phylogenetic tree.

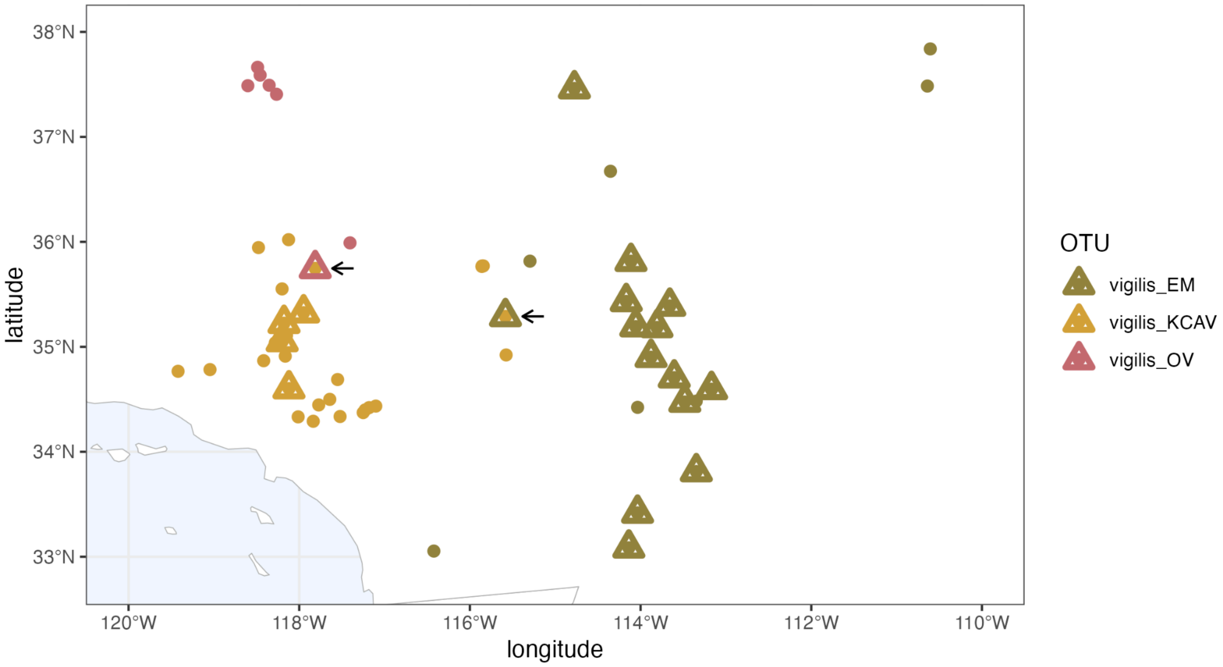

Figure S7: Geographic distribution of probable mitochondrial introgression in *Xantusia*. Individuals are colored by their operational taxonomic unit (OTU) identity based on nuclear data (circles) and mitochondrial data (triangles). Across all of *Xantusia*, we identified two possible cases of introgression, indicated by arrows. Both cases involve individuals who clustered with *X. vigilis* KCAV based on nuclear data.

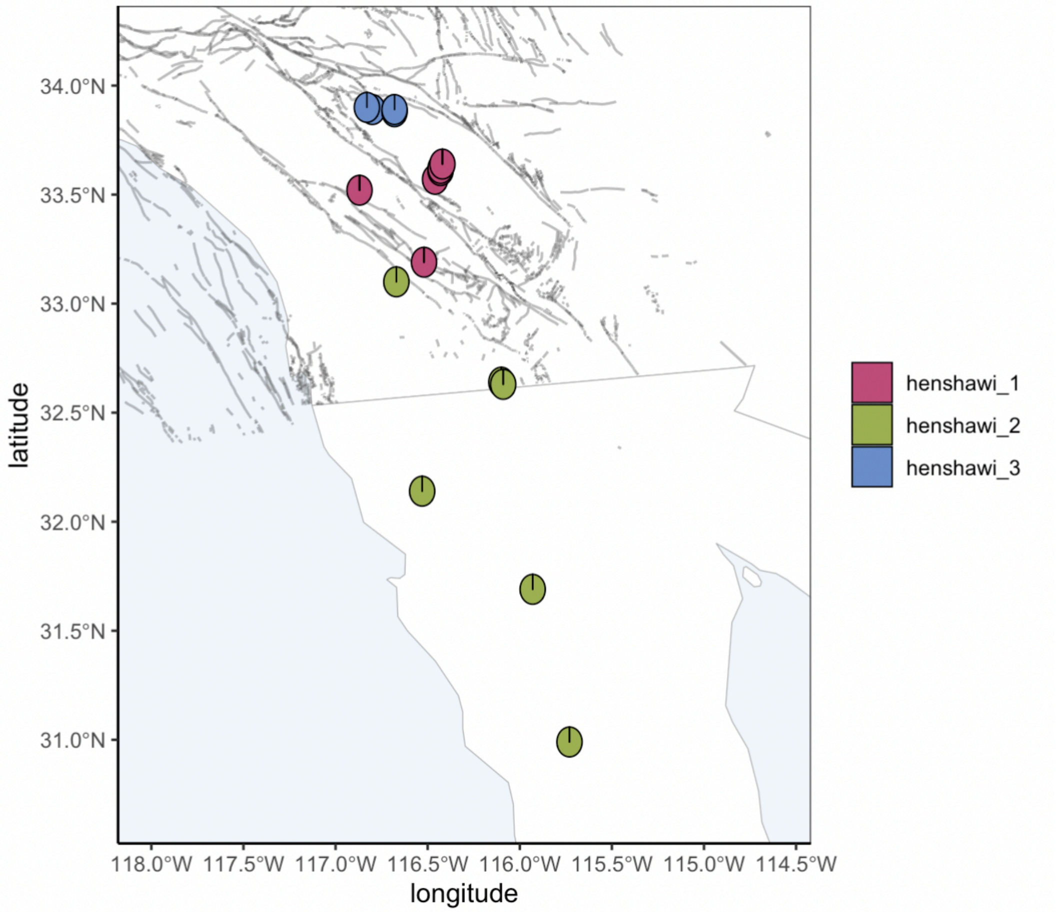

Figure S8: Geographic patterns of population clustering across one of the major clades in *Xantusia*, which consists of three operational taxonomic units (OTUs): *X. henshawi* 1, *X. henshawi* 2, *X. henshawi* 3. Each of these OTUs maps to a single genetic cluster, as determined by an ADMIXTURE analysis (see Fig. 2). For ease of visualization, pie charts illustrate the average genetic cluster probabilities for co-occurring individuals (*n* = 1 - 3). Gray lines indicate fault lines that partially separate clades; Elsinore Fault separates *X. henshawi* 1 and 2 and San Jacinto Fault isolates *X. henshawi* 3 from most of the rest of the clade. Across these three OTUs, we see no individuals with admixed ancestry.

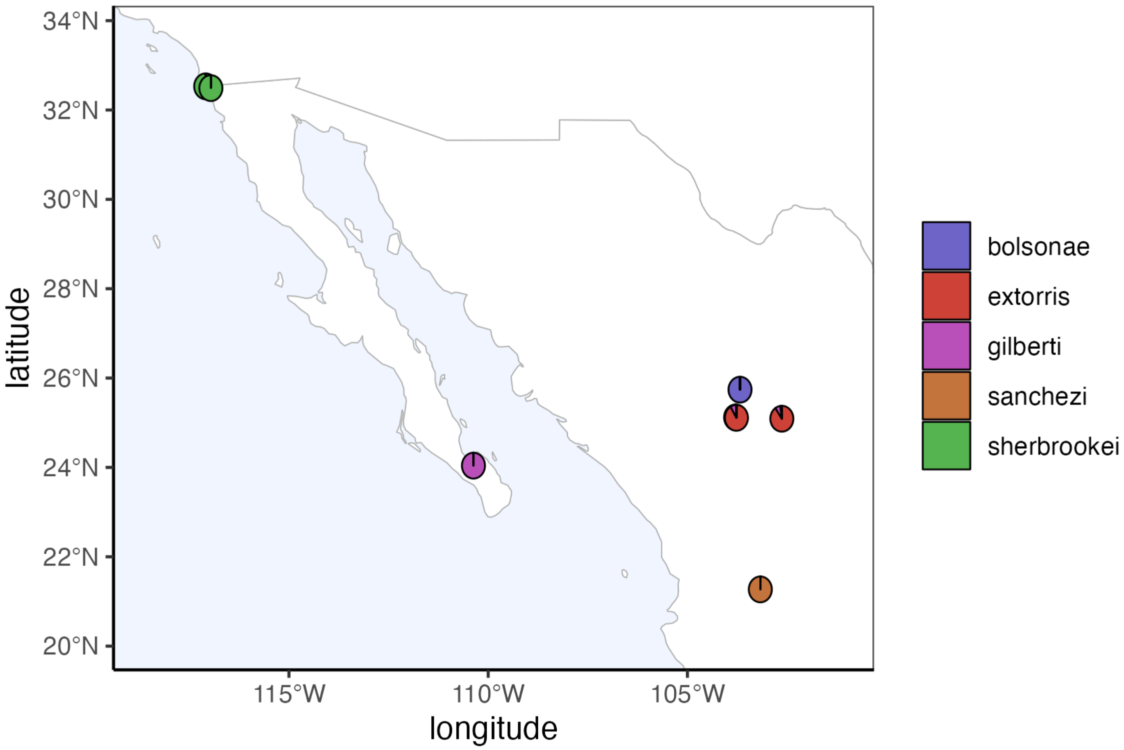

Figure S9: Geographic patterns of population clustering across one of the major clades in *Xantusia*, which consists of five operational taxonomic units (OTUs): *X. bolsonae*, *X. extorris*, *X. gilberti, X. sherbrookei,* and *X. sanchezi*. Each of these OTUs maps to a single genetic cluster, as determined by an ADMIXTURE analysis (see Fig. 2). For ease of visualization, pie charts illustrate the average genetic cluster probabilities for co-occurring individuals (*n* = 1 - 3). We see evidence for mixed ancestry in *X. extorris*. However, given the geographic distribution of the presumed ancestral populations, this mixed ancestry is unlikely due to admixture.

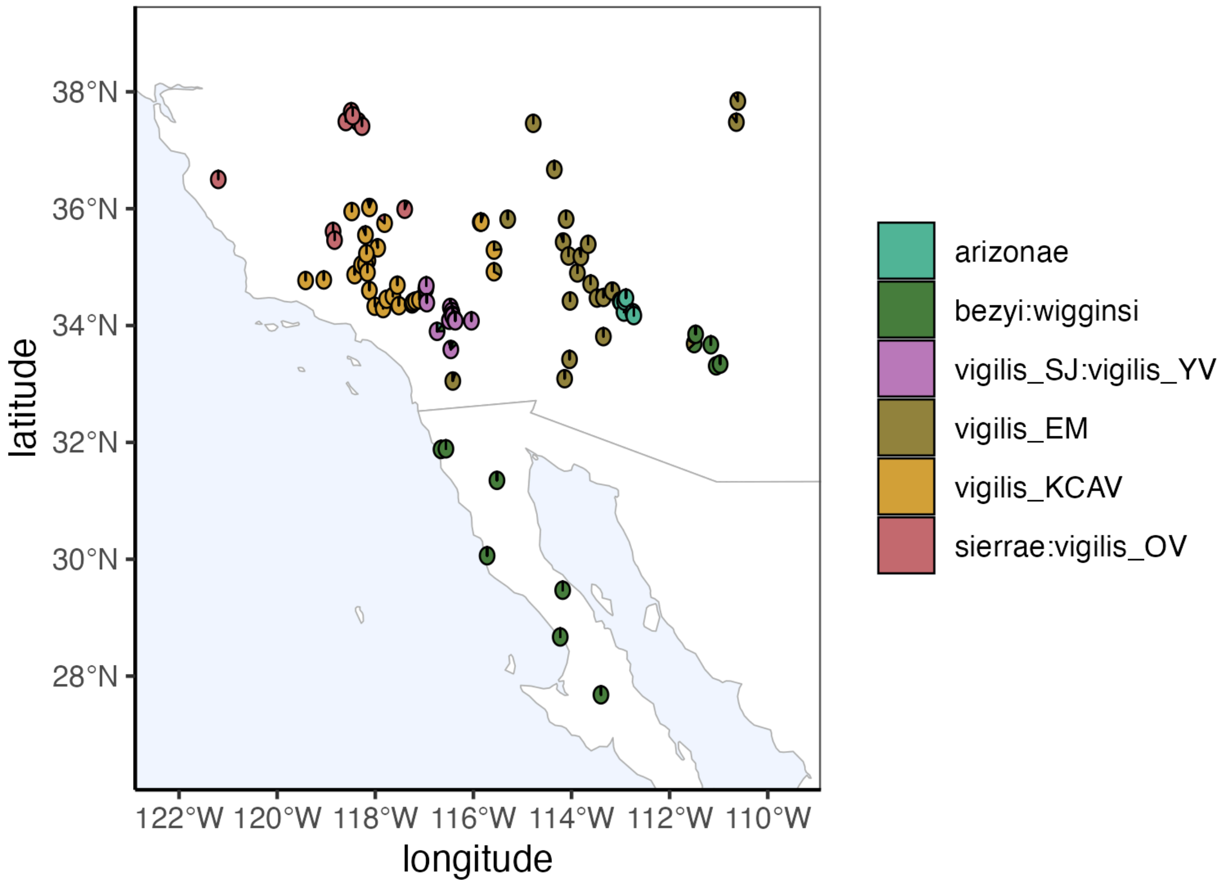

Figure S10: Geographic patterns of population clustering across one of the major clades in *Xantusia*, which consists of nine operational taxonomic units (OTUs): *X. arizonae*, *X. bezyi*, *X. sierrae, X. vigilis* EM*, X. vigilis* KCAV, *X. vigilis* OV, *X. vigilis* SJ, *X. vigilis* YV, and *X. wigginsi*. Some of these OTUs map to the same genetic cluster (*X. vigilis* SJ & *X. vigilis* YV, *X. sierrae* & *X. vigilis* OV, *X. bezyi* & *X. wigginsi*); the rest map to unique genetic clusters (see Fig. 2). For ease of visualization, pie charts illustrate the average genetic cluster probabilities for co-occurring individuals (*n* = 1 - 3). Based on the geographic distribution of individuals with mixed ancestry, there likely was admixture between *X. vigilis* EM & *X. vigilis* KCAV, *X. vigilis* KCAV & *X. vigilis* OV, and *X. vigilis* KCAV & *X. vigilis* SJ. All other individuals with mixed ancestry had unstable ancestry proportions across multiple runs of ADMIXTURE.

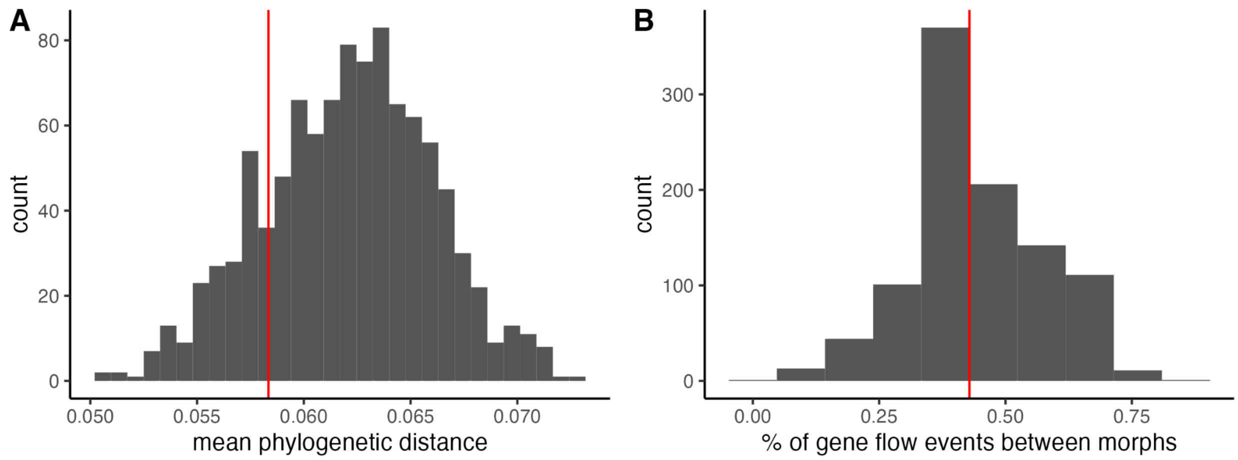

Figure S11: Introgression patterns in *Xantusia* relative to phylogenetic distance and ecomorph identity of involved pairs. Null distributions for the (**A**) mean phylogenetic distance and (**B**) percentage of pairs that are different morphs. We simulated introgression events across the phylogeny by randomly drawing two operational taxonomic units (OTUs) per clade to be a hybridizing pair. Numbers of hybridizing pairs for the three major clades were constrained to the observed data. Shown are results from 1000 simulations, along with our observed data in red. The age and ecomorph identity of our observed hybridizing pairs are no different from the null expectation.

Table S1: *Xantusia* and outgroup samples included for ddRAD sequencing in this study. Included are the original species designation (SPECIES), the museum voucher for the sample (MUSEUM), the revised operational taxonomic unit designation (OTU), geographic locality (LATITUDE & LONGITUDE) and the accession number in the Short Read Archive (SRA) hosted by NCBI. Four samples had low sequencing quality and could not be assigned to an OTU.

SAMPLE	MUSEUM	SPECIES	OTU	LATITUDE	LONGITUDE	SRA
LACM134528	LACM134528	arizonae	arizonae	34.2219365	-112.74712	SAMN41780221
LACM138275	LACM138275	arizonae	arizonae	34.2261307	-112.92725	SAMN41780235
LACM138286	LACM138286	arizonae	arizonae	34.4151237	-113.01292	SAMN41780236
LACM138847	LACM138847	arizonae	arizonae	34.1661206	-112.72943	SAMN41780242
LACM139955	LACM139955	arizonae	arizonae	34.4727099	-112.89068	SAMN41780247
LACM145119	LACM145119	arizonae	arizonae	34.4192054	-112.91704	SAMN41780253
LACM145197	LACM145197	arizonae	arizonae	34.4025	-112.989	SAMN41780259
LACM145198	LACM145198	arizonae	arizonae	34.4025	-112.989	SAMN41780260
LACM134481	LACM134481	bezyi	bezyi	33.34303	-110.9701	SAMN41780218
LACM134486	LACM134486	bezyi	bezyi	33.34303	-110.9701	SAMN41780219
LACM134498	LACM134498	bezyi	bezyi	33.8453445	-111.46763	SAMN41780220
LACM139961	LACM139961	bezyi	bezyi	33.6716637	-111.16154	SAMN41780248
LACM145111	LACM145111	bezyi	bezyi	33.3090075	-111.04706	SAMN41780252
LACM145123	LACM145123	bezyi	bezyi	33.689694	-111.50134	SAMN41780254
JLE15222	UWBM10756	bolsonae	bolsonae	25.7351944	-103.67867	SAMN41780208
JLE15223	UWBM10757	bolsonae	bolsonae	25.7351944	-103.67867	SAMN41780209
JLE15312	UWBM10765	bolsonae	bolsonae	25.7351944	-103.67867	SAMN41780213
MZFC4771	CNAR	bolsonae	bolsonae	25.1212054	-103.79271	SAMN41780318
JLE15169	UWBM10535	extorris	extorris	25.11247	-103.76997	SAMN41780205
JLE15170	UWBM10536	extorris	extorris	25.11247	-103.76997	SAMN41780206
JLE15171	UWBM10537	extorris	extorris	25.11247	-103.76997	SAMN41780207
JLE15305	UWBM10766	extorris	extorris	25.0853889	-102.63428	SAMN41780210
JLE15306	UWBM10767	extorris	extorris	25.0853889	-102.63428	SAMN41780211
JLE15311	UWBM10769	extorris	extorris	25.0853889	-102.63428	SAMN41780212
MVZ173533	MVZ173533	extorris	extorris	25.11858	-103.78942	SAMN41780282
MVZ236363	MVZ236363	extorris	extorris	25.0853333	-102.631	SAMN41780298
MZFC4764	LACM	extorris	extorris	25.1212054	-103.79271	SAMN41780317
ENEPI7701		gilberti	gilberti	24.03839	-110.37176	SAMN41780197
MVZ226109	MVZ226109	henshawi	henshawi_1	33.190371	-116.52143	SAMN41780283
MVZ232630	MVZ232630	henshawi	henshawi_1	33.5196667	-116.86967	SAMN41780287
MVZ232713	MVZ232713	henshawi	henshawi_2	33.09787	-116.66777	SAMN41780293
MVZ236369	MVZ236369	henshawi	henshawi_2	31.6865	-115.93067	SAMN41780299

MVZ236373	MVZ236373	henshawi	henshawi_2	30.9906667	-115.73	SAMN41780300
MVZ236375	MVZ236375	henshawi	henshawi_2	32.1413333	-116.52533	SAMN41780301
SD3122		henshawi	henshawi_1	33.6359	-116.41537	SAMN41780319
SD3123		henshawi	henshawi_1	33.63589	-116.41639	SAMN41780320
SD3133		henshawi	henshawi_1	33.61831	-116.42674	SAMN41780321
SD3219		henshawi	henshawi_3	33.88853	-116.68429	SAMN41780322
SD3402		henshawi	henshawi_1	33.61312	-116.42851	SAMN41780323
SDSHM68973	SDSHM68973	henshawi	henshawi_2	32.6297	-116.08916	SAMN41780324
SDSHM74951	SDSHM74951	henshawi	henshawi_3	33.87653	-116.67892	SAMN41780325
SDSNH75863	SDSNH75863	henshawi	NA	33.89459	-116.79521	SAMN41780326
SDSNH75864	SDSNH75864	henshawi	henshawi_3	33.89052	-116.7956	SAMN41780327
SDSNH75865	SDSNH75865	henshawi	henshawi_3	33.89828	-116.83417	SAMN41780328
SDSNH75866	SDSNH75866	henshawi	henshawi_3	33.90345	-116.8268	SAMN41780329
SDSNH76042	SDSNH76042	henshawi	henshawi_1	33.57327	-116.45854	SAMN41780330
XAHE05		henshawi	henshawi_2	32.63756	-116.09733	SAMN41780331
XAHE06		henshawi	henshawi_2	32.63756	-116.09733	SAMN41780332
XAHE09		henshawi	henshawi_2	32.63822	-116.09702	SAMN41780333
XAHE14		henshawi	NA	32.63767	-116.09792	SAMN41780334
XAHE18		henshawi	henshawi_2	32.63822	-116.0971	SAMN41780335
XAHE25		henshawi	henshawi_2	32.6376	-116.09789	SAMN41780336
ENEPI7707		sherbrookei	sherbrookei	32.527044	-117.089561	SAMN41780202
ENEPI7709		sherbrookei	sherbrookei	32.4928258	-116.96054	SAMN41780204
MZFC4759	CNAR	sanchezi	sanchezi	21.2669368	-103.16632	SAMN41780316
xsa373		sanchezi	sanchezi	21.2669368	-103.16632	SAMN41780337
BYU46854	BYU46854	vigilis	vigilis_EM	37.484351	-110.63943	SAMN41780195
LACM129865	LACM129865	vigilis	sierrae	35.4585203	-118.82672	SAMN41780214
LACM129875	LACM129875	vigilis	vigilis_KCAV	35.2250811	-118.17809	SAMN41780215
LACM129881	LACM129881	vigilis	vigilis_KCAV	35.9455	-118.47731	SAMN41780216
LACM134060	LACM134060	vigilis	vigilis_KCAV	35.74711	-117.81257	SAMN41780217
LACM134545	LACM134545	vigilis	vigilis_EM	35.4328473	-114.16791	SAMN41780222
LACM134557	LACM134557	vigilis	sierrae	35.6137373	-118.85839	SAMN41780223
LACM134578	LACM134578	vigilis	vigilis_KCAV	36.02064	-118.12466	SAMN41780224
LACM135194	LACM135194	vigilis	vigilis_EM	35.1846997	-113.80801	SAMN41780225
LACM135205	LACM135205	vigilis	vigilis_EM	35.8153536	-114.11246	SAMN41780226
LACM135374	LACM135374	vigilis	vigilis_KCAV	35.3255905	-117.94844	SAMN41780227
LACM136235	LACM136235	vigilis	vigilis_KCAV	35.0384367	-118.28023	SAMN41780228
LACM136734	LACM136734	vigilis	vigilis_KCAV	37.90708	-110.57433	SAMN41780229

LACM137433	LACM137433	vigilis	vigilis_KCAV	34.6017522	-118.12025	SAMN41780231
LACM137438	LACM137438	vigilis	vigilis_KCAV	34.78299	-119.04547	SAMN41780232
LACM138247	LACM138247	vigilis	vigilis_KCAV	34.9111414	-118.16349	SAMN41780233
LACM138254	LACM138254	vigilis	vigilis_KCAV	34.49944	-117.64197	SAMN41780234
LACM138298	LACM138298	vigilis	vigilis_EM	34.5948	-113.16889	SAMN41780237
LACM138825	LACM138825	vigilis	vigilis_EM	35.192739	-114.05604	SAMN41780238
LACM138827	LACM138827	vigilis	vigilis_EM	34.9006679	-113.87738	SAMN41780239
LACM138837	LACM138837	vigilis	vigilis_EM	33.0851295	-114.1375	SAMN41780240
LACM138840	LACM138840	vigilis	vigilis_EM	33.4168683	-114.0356	SAMN41780241
LACM139927	LACM139927	vigilis	vigilis_EM	34.5948	-113.16889	SAMN41780243
LACM139936	LACM139936	vigilis	vigilis_EM	34.705729	-113.60555	SAMN41780244
LACM139942	LACM139942	vigilis	vigilis_EM	35.3890993	-113.65772	SAMN41780245
LACM139947	LACM139947	vigilis	NA	35.3890993	-113.65772	SAMN41780246
LACM145078	LACM145078	vigilis	NA	37.32517	-118.53443	SAMN41780249
LACM145086	LACM145086	vigilis	vigilis_KCAV	35.0511682	-118.1998	SAMN41780251
LACM145140	LACM145140	vigilis	vigilis_EM	37.4605395	-114.77537	SAMN41780255
LACM145148	LACM145148	vigilis	vigilis_EM	36.67234	-114.35255	SAMN41780256
LACM145156	LACM145156	vigilis	vigilis_EM	35.8160434	-115.29616	SAMN41780257
LACM145170	LACM145170	vigilis	vigilis_EM	34.4741667	-113.48183	SAMN41780258
LACM145210	LACM145210	vigilis	vigilis_EM	33.8119974	-113.34682	SAMN41780261
LACM151489	LACM151489	vigilis	vigilis_KCAV	35.2899189	-115.58326	SAMN41780262
LACM183106	LACM183106	vigilis	vigilis_KCAV	35.76888	-115.85587	SAMN41780263
LACM183109	LACM183109	vigilis	vigilis_KCAV	35.7709	-115.85471	SAMN41780264
LACM184722	LACM184722	vigilis	vigilis_OV	35.99034	-117.40487	SAMN41780265
LACM186656	LACM186656	vigilis	vigilis_KCAV	34.92227	-115.5755	SAMN41780266
LACM186759	LACM186759	vigilis	vigilis_KCAV	34.29079	-117.83568	SAMN41780267
LACM186762	LACM186762	vigilis	vigilis_KCAV	34.688347	-117.55008	SAMN41780268
LACM186805	LACM186805	vigilis	vigilis_KCAV	34.33259	-118.01248	SAMN41780269
LACM186943	LACM186943	vigilis	vigilis_KCAV	35.10905	-118.14864	SAMN41780270
LACM187025	LACM187025	vigilis	vigilis_KCAV	35.77083	-115.84325	SAMN41780271
LACM187026	LACM187026	vigilis	vigilis_KCAV	35.76559	-115.85992	SAMN41780272
LACM187136	LACM187136	vigilis	vigilis_OV	37.40599	-118.26578	SAMN41780273
LACM187162	LACM187162	vigilis	vigilis_OV	37.49185	-118.3522	SAMN41780274
LACM188013	LACM188013	vigilis	vigilis_OV	37.66303	-118.4876	SAMN41780275
LACM188014	LACM188014	vigilis	vigilis_OV	37.58829	-118.45799	SAMN41780276
LACM189193	LACM189193	vigilis	vigilis_OV	37.4876	-118.60206	SAMN41780277
MVZ137517	MVZ137517	vigilis	vigilis_KCAV	35.5516298	-118.2008	SAMN41780281

MVZ229114	MVZ229114	vigilis	vigilis_KCAV	34.8676418	-118.41638	SAMN41780284
MVZ231865	MVZ231865	vigilis	vigilis_EM	37.8381667	-110.60517	SAMN41780285
MVZ232572	MVZ232572	vigilis	vigilis_EM	34.4826667	-113.34767	SAMN41780286
MVZ232636	MVZ232636	vigilis	vigilis_SJ	33.5855	-116.45533	SAMN41780288
MVZ232652	MVZ232652	vigilis	vigilis_EM	34.4233333	-114.035	SAMN41780289
MVZ232653	MVZ232653	vigilis	vigilis_YV	34.0846667	-116.3735	SAMN41780290
MVZ232658	MVZ232658	vigilis	vigilis_SJ	34.0875	-116.49283	SAMN41780291
MVZ232669	MVZ232669	vigilis	vigilis_KCAV	34.76687	-119.41957	SAMN41780292
MVZ232719	MVZ232719	vigilis	sierrae	36.4993333	-121.205	SAMN41780294
MVZ232723	MVZ232723	vigilis	vigilis_KCAV	34.336	-117.52133	SAMN41780295
MVZ232726	MVZ232726	vigilis	vigilis_EM	33.054	-116.42233	SAMN41780296
MVZ232731	MVZ232731	vigilis	vigilis_SJ	33.8992	-116.74467	SAMN41780297
MVZ249130	MVZ249130	vigilis	vigilis_YV	34.15514	-116.41901	SAMN41780302
MVZ249136	MVZ249136	vigilis	vigilis_YV	34.24404	-116.43578	SAMN41780303
MVZ249137	MVZ249137	vigilis	vigilis_YV	34.17918	-116.42757	SAMN41780304
MVZ250600	MVZ250600	vigilis	vigilis_YV	34.3143333	-116.47483	SAMN41780305
MVZ250603	MVZ250603	vigilis	vigilis_YV	34.387	-116.94617	SAMN41780306
MVZ250605	MVZ250605	vigilis	vigilis_YV	34.6761667	-116.96367	SAMN41780307
MVZ250606	MVZ250606	vigilis	vigilis_YV	34.63	-116.96567	SAMN41780308
MVZ250610	MVZ250610	vigilis	vigilis_KCAV	34.435285	-117.10267	SAMN41780309
MVZ250613	MVZ250613	vigilis	vigilis_KCAV	34.420874	-117.18121	SAMN41780310
MVZ250614	MVZ250614	vigilis	vigilis_KCAV	34.3986667	-117.22733	SAMN41780311
MVZ250619	MVZ250619	vigilis	vigilis_KCAV	34.3733333	-117.25033	SAMN41780312
MVZ250620	MVZ250620	vigilis	vigilis_KCAV	34.4461667	-117.7715	SAMN41780313
MVZ250622	MVZ250622	vigilis	vigilis_YV	34.0801667	-116.03583	SAMN41780314
MVZ250734	MVZ250734	vigilis	vigilis_YV	34.0896667	-116.37867	SAMN41780315
ENEPI7700		wigginsi	wigginsi	31.35487	-115.52311	SAMN41780196
ENEPI7702		wigginsi	wigginsi	31.884065	-116.662	SAMN41780198
ENEPI7703		wigginsi	wigginsi	29.4691702	-114.17604	SAMN41780199
ENEPI7704		wigginsi	wigginsi	30.0601054	-115.72494	SAMN41780200
ENEPI7706		wigginsi	wigginsi	31.8905593	-116.56374	SAMN41780201
ENEPI7708		wigginsi	wigginsi	28.6698867	-114.23428	SAMN41780203
LACM136799	LACM136799	wigginsi	wigginsi	27.67659	-113.4037	SAMN41780230
LACM145080	LACM145080	wigginsi	wigginsi	27.67659	-113.4037	SAMN41780250
UTAR38021		L. mayae	NA	NA	NA	SAMN41780278
LACM131145	LACM131145	L. sylvaticum	NA	NA	NA	SAMN41780279
LACM136352	LACM136352	L. tuxtlae	NA	NA	NA	SAMN41780280

Table S2: Model fit (as measured by Akaike Information Criterion [AIC]) for different models of trait evolution. Here, we modeled the transition between plant ecomorph and rock ecomorph in *Xantusia*. The best fitting model is the equal-rates model though the unidirectional model 1 also has some support.

Model	Model description	Log-likelihood	AIC
Equal-rates model (ER)	Rates between both transition types are equal	-13.01470	28.02941
All rates different (ARD)	Rates between both transition types are different	-13.01470	30.02941
Unidirectional model 1	Species only transition from plant to rock ecomorphs	-13.20358	28.40716
Unidirectional model 2	Species only transition from rock to plant ecomorphs	-16.87605	35.75209

Table S3: Differences between recognized species and operational taxonomic units (OTUs). Revising our taxonomy led to *Xantusia henshawi* being split into 3 OTUs and *X. vigilis* being split into 5 OTUs. Below we explore how these different species delimitations affect our understanding of species geography, genetics, and morphology. For species, we report the values for each measured trait; for OTUs, we report the mean and its range. Crown age is given in relative units; the maximum age of the tree is 0.074. Across most metrics, OTUs exhibit significantly reduced range size, genetic diversity, genetic differentiation, and crown age relative to species.

	Xantusia henshawi		*Xantusia vigilis*	
	sensu stricto	OTU	*sensu stricto*	OTU
Number of taxa	1	3	1	5
Monophyletic?	yes	for all OTUs, yes	no	for 4 OTUs, yes
Geographic range size	19326 km^2	5326 km^2 (668–12555)	312359 km^2	47663 km^2 (2285–168702)
Genetic diversity (π)	0.00668	0.00238 (0.00134–0.00351)	0.00608	0.002814 (0.00226–0.00338)
Between individual F_{ST}	0.61 (-0.22–0.90)	0.29 (-0.21–0.79)	0.59 (-0.83–0.90)	0.41 (-0.83–0.84)
Crown age	0.054	0.032 (0.027–0.042)	0.062	0.023 (0.012–0.048)
Any evidence of ecomorph transition?	All rock ecomorph	All rock ecomorph	All plant ecomorph	All plant ecomorph